

## DEPTH CONCENTRATIONS OF DEUTERIUM IONS IMPLANTED INTO SOME PURE METALS AND ALLOYS

*A. Yu. Didyk*<sup>a, 1</sup>, *R. Wiśniewski*<sup>b, 2</sup>, *K. Kitowski*<sup>b, 3</sup>,  
*V. Kulikauskas*<sup>c, 4</sup>, *T. Wilczynska*<sup>b, 5</sup>, *A. Hofman*<sup>b</sup>,  
*A. A. Shiryaev*<sup>d, 6</sup>, *Ya. V. Zubavichus*<sup>e</sup>

<sup>a</sup> Joint Institute for Nuclear Research, Dubna

<sup>b</sup> Institute of Atomic Energy POLATOM, Otwock/Świerk, Poland

<sup>c</sup> Skobeltsyn Institute of Nuclear Physics of Moscow State University, Moscow

<sup>d</sup> Institute of Physical Chemistry and Electrochemistry of RAS, Moscow

<sup>e</sup> Russian Research Center «Kurchatov Institute», Moscow

Pure metals (Cu, Ti, Zr, V, Pd) and diluted Pd alloys (Pd–Ag, Pd–Pt, Pd–Ru, Pd–Rh) were implanted by 25-keV deuterium ions at fluences in the range  $(1.2–2.3) \cdot 10^{22} \text{ m}^{-2}$ . The post-treatment depth distributions of deuterium ions were measured 10 days and three months after the implantation by using Elastic Recoil Detection Analysis (ERDA) and Rutherford Backscattering (RBS). Comparison of the obtained results allowed us to make conclusions about relative stability of deuterium and hydrogen gases in pure metals and diluted Pd alloys. Very high diffusion rates of implanted deuterium ions in V and Pd pure metals and Pd alloys were observed. Small-angle X-ray scattering revealed formation of nanosized defects in implanted corundum and titanium.

Образцы чистых металлов (Cu, Ti, Zr, V, Pd) и разбавленных сплавов Pd были имплантированы ионами дейтерия с энергией 25 кэВ до флюенсов в интервале  $(1,2–2,3) \cdot 10^{22} \text{ м}^{-2}$ . Исследования образцов с помощью метода регистрации ядер отдачи и резерфордского обратного рассеяния были проведены спустя 10 суток и три месяца после имплантации. Сравнение полученных результатов позволило сделать выводы об относительной стабильности имплантированного дейтерия и водорода в вышеперечисленных сплавах. Было показано, что в образцах V, Pd и Pd-сплавов наблюдаются высокие значения коэффициентов диффузии. Использование малоуглового рассеяния рентгеновских лучей позволило выявить присутствие наноразмерных кластеров (дефектов) в имплантированном корунде и титане.

PACS: 25.45.-z

---

<sup>1</sup>E-mail: didyk@jinr.ru

<sup>2</sup>E-mail: roland.wisniewski@gmail.com

<sup>3</sup>E-mail: kacper.co@gmail.com

<sup>4</sup>E-mail: vaclav@anna19.sinp.msu.ru

<sup>5</sup>E-mail: teresa.wilczynska@gmail.com

<sup>6</sup>E-mail: a\_shiryaev@mail.ru

## INTRODUCTION

Behavior of hydrogen isotopes in solids is of considerable fundamental and applied interest. Hydrogen-based energetics is a viable alternative to modern hydrocarbon-based technologies. One of the promising approaches involves hydrogen stored in metal hydrides [1–4]. Hydrogen and its heavier isotopes serve as a nuclear fuel in fusion reactor power plants [5–9]. They are also widely used in modern nuclear reactors for slowing-down of neutrons, and as neutrons reflectors-mirrors, as safety materials and in the regulatory systems [7]. Production of high neutron fluxes for various applications remains an important challenge. The increase of capacity of metal foils to retain deuterium in the near-surface layers is another important problem. The basic challenge in all these applications is to achieve the highest possible hydrogen concentration in the employed materials preserving, at the same time, the capability of desorbing hydrogen reversibly. Materials with high deuterium concentrations are important for some nuclear applications, such as neutron sources.

Ion implantation is one of the possible ways to create high hydrogen concentrations in the subsurface layers. In this work we report some results of research into the behavior of deuterium in various pure metals and alloys. We have studied in detail depth distribution of implanted deuterium and temporal stability of the implanted layers (for review of previous studies, see [8–13] and references therein). We have monitored evolution of hydrogen and deuterium concentrations after long-term saturation of pure palladium and its diluted alloys. Finally, the maximal stable concentrations of implanted deuterium ions in the metals and chemical compounds were estimated and compared with maximum equilibrium relations between metals and hydrogen (for example, comparison with metal hydrides such as  $\text{TiH}_2$ ,  $\text{MgH}_2$ ,  $\text{AlH}_3$  [7]).

### 1. EXPERIMENTAL METHODS AND SAMPLE PREPARATION

All samples of metals (purity of about 99.95%) were prepared by mechanical polishing and then by electrochemical etching to achieve high-quality smooth surfaces. Surface structures were studied using optical microscopy (metallographic optical microscope «Neophot», MOM), scanning electron microscopy (JSM-840, SEM), and atomic force microscopy (AFM) prior to the implantation to check the homogeneity.

Single crystal ingots of Pd and Pd alloys were grown at the Institute of Atomic Energy (Świerk, Poland). The ingots were cut to thickness about 1–2 mm. Then the samples were cold rolled, and finally mechanically and electrochemically polished to the final thickness of 50–150  $\mu\text{m}$ . For every compound four specimens were prepared. The first set was saturated by deuterium in a high-pressure chamber [14, 15]; the second part was implanted by  $\text{D}^+$  ions up to high fluences. The third and fourth samples were annealed at a temperature of about 900 K for 1 hour and then were deuterium saturated (the third specimen) and implanted up to the same ion fluences (the fourth).

**1.1. Implantation of 25-keV  $\text{D}^+$  Ions at High Fluences.** The implantation of 25-keV deuterium ions was carried out at dedicated low-energy ion irradiation beamline equipped with a separation magnet, deviation systems in both vertical and horizontal directions, and a number of flux-measuring Faraday cups in both directions [16]. Homogeneity of irradiation in a square of about  $6 \times 4$  cm was better than  $\pm 5\%$ . All samples were glued by a heat conducting glue to a cooling substrate and the temperature of implantation was  $T \approx 30^\circ\text{C}$ . It is necessary to note that the ion beam flux during the implantation was about  $35 \cdot 10^{17} \text{ m}^{-2} \cdot \text{s}^{-1}$ , and

the beam power was less than  $W \approx 0.075 \text{ W/cm}^2$ . Maximum implantation fluence in all targets was  $\Phi_{\text{max}} = 2.3 \cdot 10^{22} \text{ m}^{-2}$  to exclude surface phenomena such as blistering and exfoliation as observed by optical and electron microscopies. Duration of the implantation for this maximum  $\text{D}^+$  fluence was about 20 h. All metal samples and alloys were irradiated up to four ion fluences, i.e.,  $\Phi_1 = 1.2 \cdot 10^{22}$ ,  $\Phi_2 = 1.5 \cdot 10^{22}$ ,  $\Phi_3 = 1.8 \cdot 10^{22}$ , and  $\Phi_{\text{max}} = 2.3 \cdot 10^{22} \text{ m}^{-2}$ . Atomic force microscopy (AFM) was used for estimations of surface sputtering rates of all samples. The post-experimental metal surface roughness was comparable to calculations of the surface sputtering with computer code SRIM-2008 [17]. It is necessary to note that all implanted metal samples were deformed by a spontaneous emergence of gas pores or gas bubbles (so-called swelling processes). There was a surface discoloration with intensity depending on the ion implantation fluence.

**1.2. Depth Distribution of Implanted  $\text{D}^+$  Ions in Various Materials: Elastic Recoil Detection Analysis (ERDA-RBS).** The depth distribution of implanted  $\text{D}^+$  ions was measured using RBS setup based on electrostatic generator (EG-5) of the Frank Laboratory of Neutron Physics (FLNP, JINR, Dubna) [19] and tandetron at the Skobeltsyn Institute of Nuclear Physics (SINP, MSU, Moscow) [21]. Concentration profiles of light H/D atoms were measured by elastic recoil detection analysis (ERDA). The depth distributions of chemical complex compounds, such as diluted Pd alloys,  $\text{Al}_2\text{O}_3$  and stainless steel ( $\text{Fe}_{72}\text{Cr}_{18}\text{Ni}_{10}$  — SS) were measured by RBS [19–21]. We have employed 2.3-MeV  $\text{He}^+$ , the incidence angle was  $\alpha = 15^\circ$ . Registration of scattering hydrogen and deuterium recoils was performed at  $30^\circ$  to an initial  $\text{He}^+$  beam direction. The beamspot on the sample was elliptical with axes of  $a_1 \approx 1 \text{ mm}$  and  $a_2 \approx 3.9 \text{ mm}$ . All experimental spectra were then fitted with SIMNRA 6.05. The experimental ERDA and simulated spectra of H and D recoils under analysis by  $\text{He}^+$  ions with an energy of 1.9 MeV for  $\text{Pd}_{0.9}\text{Pt}_{0.1}$  alloy implanted by deuterium ions with an energy of 25 keV at fluence  $\Phi_1 = 1.2 \cdot 10^{22} \text{ m}^{-2}$  versus the number of energetic channels are presented in Fig. 1. Here the sliding angle to the surface is  $\alpha = 15^\circ$  and the angle of recoil registration to the direction of  $\text{He}^+$  ions is  $\theta = 30^\circ$ . The thickness of  $\text{He}^+$  ion adsorption mylar foil was  $12 \mu\text{m}$ .

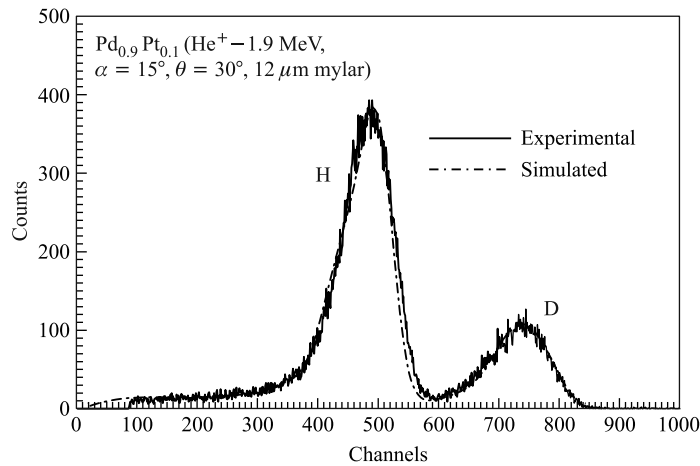


Fig. 1. The experimental ERDA and simulated spectra of H and D recoils in  $\text{Pd}_{0.9}\text{Pt}_{0.1}$  alloy implanted by 25-keV deuterium ions up to fluence  $\Phi_1 = 1.2 \cdot 10^{22} \text{ m}^{-2}$

**1.3. X-ray Investigations of the Samples.** The X-ray diffraction patterns were acquired from the Pd alloys foils in reflection geometry using X'Pert Panalytical powder diffractometer. It is not surprising that the thickness of the implanted layers was too small to be detected. The main result of the diffraction experiments is the observation of texture, imposed by cold rolling of the samples.

Small-angle X-ray scattering (SAXS) patterns were acquired at the STM beamline [27] at the Kurchatov synchrotron source using linear position-sensitive detector. Relatively high energy of incident monochromatic radiation (15–17 keV) was employed to permit recording of the patterns in transmission geometry. The samples were in vacuum. The size distribution of the scatterers was calculated in the assumption of spherical shape using GNOM software [28]. Comparison with unimplanted samples showed that the texture of the samples was not important for the scattering and the analyzed signal is due to defects due to implanted/infused hydrogen.

## 2. EXPERIMENTAL RESULTS

### 2.1. Depth Distribution of Implanted D<sup>+</sup> Ions in Some Pure Metals and Some Alloys.

Table 1 presents the most important calculated parameters for D<sup>+</sup> (25 keV) and for analyzing He<sup>+</sup> (2.3 MeV) ions. Namely, mass and atomic densities, projected ranges of D<sup>+</sup> and He<sup>+</sup> ions and sputtering coefficients of all the metals and chemical compounds studied are given. The concentration profile of ions implanted into a target can be calculated using the expression (see [21, 22])

$$C(Z) = \frac{N_0}{2 \times S} \left[ \operatorname{erf} \left( \frac{Z + \frac{\Phi \times S}{N_0} - R_p}{\sqrt{2} \times \Delta R_p} \right) - \operatorname{erf} \left( \frac{Z - R_p}{\sqrt{2} \times \Delta R_p} \right) \right], \quad (1)$$

here  $N_0$  is atomic target density (at · cm<sup>3</sup>);  $\Phi$  is ion fluence (cm<sup>-2</sup>);  $S$  is sputtering coefficient for target atoms;  $R_p$  and  $\Delta R_p$  are projected range and straggling of ions in target. The total

*Table 1. Calculated (SRIM-2008 [17]) parameters for all the studied compounds*

| Material   | Zr         | Ti         | Cu          | V          | Pd          | SS                                     | Al <sub>2</sub> O <sub>3</sub> |
|--|------------|------------|-------------|------------|-------------|--|--------------------------------|
| Implantation of 25-keV deuterium ions                            |            |            |             |            |             |  |                                |
| $\rho$ ,<br>g/cm <sup>3</sup>                                    | 6.49       | 4.519      | 8.92        | 5.96       | 12.03       | 7.849                                  | 3.5                            |
| $N$ ,<br>10 <sup>22</sup> at. M/cm <sup>3</sup>                  | 4.284      | 5.681      | 8.453       | 7.045      | 6.803       | 8.526                                  | 10.33                          |
| $R_p^D$ , Å  | 1923 ± 643 | 2444 ± 695 | 1854 ± 673  | 1955 ± 571 | 1237 ± 458  | 1998 ± 698                             | 1923 ± 643                     |
| $S$ ,<br>at. M/at. D   | 0.00248    | 0.0019     | 0.010       | 0.0025     | 0.0011      | 0.0012(Cr)<br>0.0007(Ni)<br>0.0049(Fe) | 0.00153(Al)<br>0.0024(O)       |
| Analyzing 2.3-MeV helium ions, grazing angle $\alpha = 15^\circ$ |            |            |             |            |             |  |                                |
| $R_p^D$ ,<br>μm  | 1.32       | 1.43       | 1.07 ± 0.33 | 1.04       | 0.88 ± 0.30 | 0.95 ± 0.26                            | 1.38                           |

implantation dose can be calculated using expression (1) as

$$C_D = \int_0^{\infty} C(Z) dZ \approx \sum_{i=1}^{i=i_{\max}} C_i \times \Delta Z_i, \quad (2)$$

and the maximum ion concentration should be

$$C^{\max} = \frac{N_0}{S} \times \operatorname{erf} \left[ \frac{\Phi \cdot S}{2\sqrt{2}N_0\Delta R_p} \right] \quad (3)$$

at the depth  $Z_{\max} = R_p - \frac{\Phi \cdot S}{2N_0}$ .

*2.1.1. Implantation to Zr Target.* The depth-dependent concentrations of D and H (intrinsic impurity) at two implantation fluences  $\Phi_2 = 1.5 \cdot 10^{22} \text{ m}^{-2}$  and  $\Phi_{\max} = 2.3 \cdot 10^{22} \text{ m}^{-2}$  for Zr samples are presented in Fig. 2. Integral concentrations of the implanted ions can be introduced

using simple expressions  $c_{D,H} \equiv \sum_{i=1}^{i_{\max}} c_i(D,H) \times \Delta Z_i$ , where indices «*i*» correspond to depth layers in a target from  $Z = 0$  up to maximum ERDA measured depth  $Z < R_p^{\text{He}}$ . As is seen from Table 1, the projected range of D ions in Zr foil is equal to  $R_p^D = (1923 \pm 643) \text{ \AA}$ . By using the sputtering coefficient  $S_{Zr} = 2.48 \cdot 10^{-3} \text{ at. Zr/at. D}^+$ , it is very easy to estimate the thickness of the surface layer sputtered by implantation of  $D^+$  at a fluence of  $\Phi_{\max} = 2.3 \cdot 10^{22} \text{ m}^{-2}$  to be equal to  $\Delta Z = \Phi_{\max} \times S_{Zr}/N_{Zr} = 13.3 \text{ \AA}$ .

Figure 2 shows that: a) the depth concentrations of D atoms for all fluences have a very large spread along the implanted ion path and the width of implanted zone is much larger than the projected range  $R_p^D = (1923 \pm 643) \text{ \AA}$ ; b) the total concentrations of D atoms correspond closely to the experimental ion fluences for Zr targets only; c) the maximum obtained

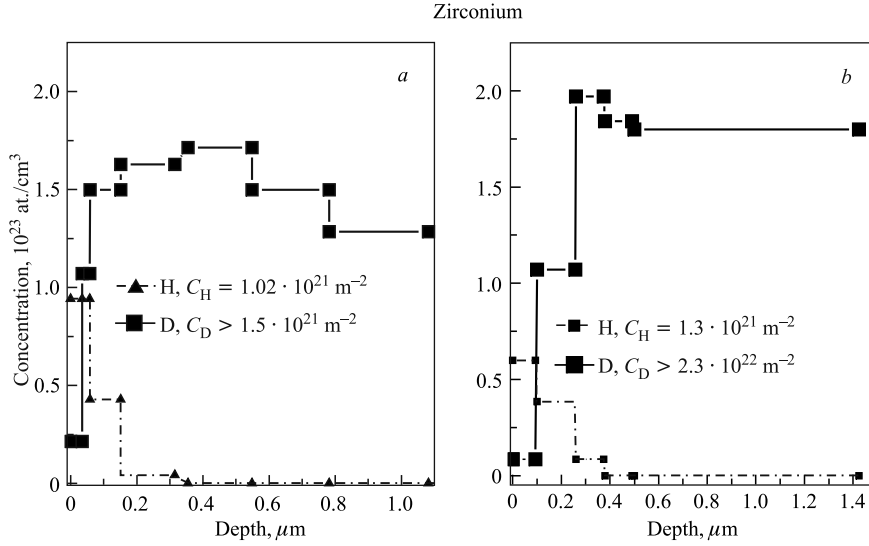


Fig. 2. The depth profiles of D and H atoms in Zr samples after 25-keV  $D^+$  implantation at two fluences:  $\Phi_2 = 1.5 \cdot 10^{22} \text{ m}^{-2}$  (a) and  $\Phi_{\max} = 2.3 \cdot 10^{22} \text{ m}^{-2}$  (b). Concentrations of the isotopes are given. The  $D^+$  ion projected range is  $R_p = (1923 \pm 643) \text{ \AA}$

concentration of D atoms in Zr is about 47%, i.e.,  $n_{\text{Zr}}^{\text{exp}}(\text{D}^+) = 0.47 \text{ at. D/at. Zr} < n_{\text{Zr}}^{\text{max}} = 2.95 \text{ at. D/at. Zr}$ . Here  $n_{\text{Zr}}^{\text{max}}(\text{D}^+) = 2.95 \text{ at. D/at. Zr}$  is the calculated deuterium–metal ratio for maximum fluence of implantation, i.e.,  $n^{\text{max}} \equiv C^{\text{max}}/N_0$ . The calculated profiles and other parameters were obtained using SRIM-2008 simulation [17] (depth profiles,  $R_p$ ,  $\Delta R_p$  and  $N_0$ ) and using homemade computer program SPECTR based on expressions (1)–(3).

**2.1.2. Implantation to Ti Target.** The measured depth distributions of D and H atoms in implanted Ti samples (ion fluences  $\Phi_3 = 1.8 \cdot 10^{22} \text{ m}^{-2}$  and  $\Phi_{\text{max}} = 2.3 \cdot 10^{22} \text{ m}^{-2}$ ) are presented in Fig. 3. *In contrast to implantation to Zr metal, the integral concentration of implanted deuterium is lower due to larger projected range (see Table 1). This could be the reason for wider spread of the profiles.*

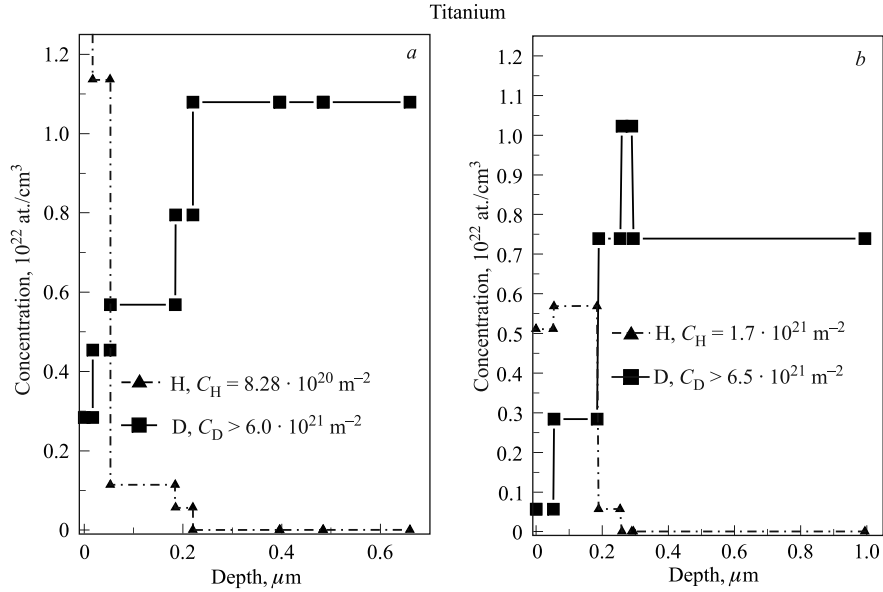


Fig. 3. The depth profiles of D and H atoms in Ti samples after 25-keV  $\text{D}^+$  implantation at two fluences:  $\Phi_2 = 1.8 \cdot 10^{22} \text{ m}^{-2}$  (a) and  $\Phi_{\text{max}} = 2.3 \cdot 10^{22} \text{ m}^{-2}$  (b). The  $\text{D}^+$  projected range is  $R_p = (2446 \pm 493) \text{ \AA}$

**2.1.3. Implantation to  $\text{Al}_2\text{O}_3$  Target.** The total concentration of deuterium implanted into synthetic  $\text{Al}_2\text{O}_3$  single crystal is shown in Fig. 4. These crystals possessed high surface quality as shown by AFM. The use of ERDA technique with relatively low projected range of  $\text{He}^+$  (2.3 MeV) ions and small thickness of implanted layers required a smooth surface. It is easy to see from Fig. 4 that: a) the depth distributions of implanted  $\text{D}^+$  ions for fluence  $\Phi_{\text{max}} = 2.3 \cdot 10^{22} \text{ m}^{-2}$  have a very big spread along the implanted ion path and the width of implanted zone is much larger than the projected range  $R_p^{\text{D}} = (2832 \pm 602) \text{ \AA}$ ; b) the integral concentration of D atoms exceeds  $C_{\text{D}} > 6.43 \cdot 10^{21} \text{ m}^{-2}$ ; c) the maximum measured concentration of D atoms in  $\text{Al}_2\text{O}_3$  sample is about 15%, i.e.,  $n_{\text{Al}_2\text{O}_3}^{\text{exp}}(\text{D}^+) = 0.15 \text{ at. D/at. Al}_2\text{O}_3 \ll n_{\text{Al}_2\text{O}_3}^{\text{max}} = 1.69 \text{ at. D/at. Al}_2\text{O}_3$ . Here  $n_{\text{Al}_2\text{O}_3}^{\text{max}} = 1.69 \text{ at. D/at. Al}_2\text{O}_3$  is the calculated deuterium/ $\text{Al}_2\text{O}_3$  ratio for the maximal implantation fluence. The maximum concentrations of D atoms were achieved at the depths between 0.26 and 0.4  $\mu\text{m}$ . This depth region is comparable with the projected range of  $\text{D}^+$  ions in  $\text{Al}_2\text{O}_3$  sample  $R_p^{\text{D}} = (0.28 \pm 0.06) \mu\text{m}$ .

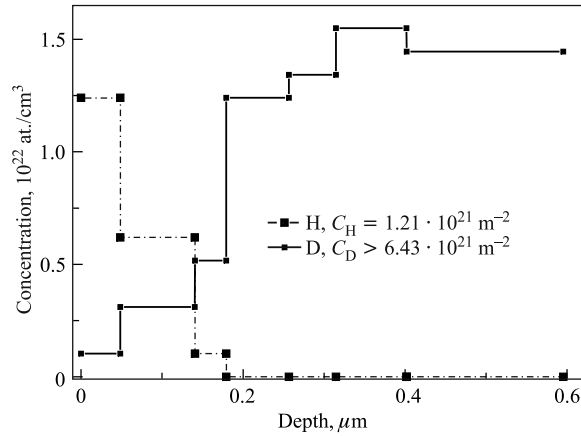


Fig. 4. The depth profiles of D and H atoms in  $\text{Al}_2\text{O}_3$  single crystal after 25-keV  $\text{D}^+$  implantation at fluence  $\Phi_{\text{max}} = 2.3 \cdot 10^{22} \text{ m}^{-2}$ . The  $\text{D}^+$  projected range is  $R_p = (2832 \pm 602) \text{ \AA}$

The experimental low value of the deuterium/ $\text{Al}_2\text{O}_3$  ratio can be explained by a high spread of the implantation layer, larger than the analyzed  $\text{He}^+$  ion projected range. It is necessary to check this conclusion by another method sensitive to deuterium depth distribution, e.g., by secondary mass ion spectrometry.

**2.1.4. Implantation to Copper and Stainless Steel Targets.** Figure 5 shows the depth profiles of D and H atoms in copper and stainless steel ( $\text{Fe}_{72}\text{Cr}_{18}\text{Ni}_{10}$ ) samples at the  $\text{D}^+$  fluence  $\Phi_2 = 1.5 \cdot 10^{22} \text{ m}^{-2}$  as measured by ERDA. One can conclude that the total D concentration and shape of the depth profiles in these samples are similar to the titanium ones (see above).

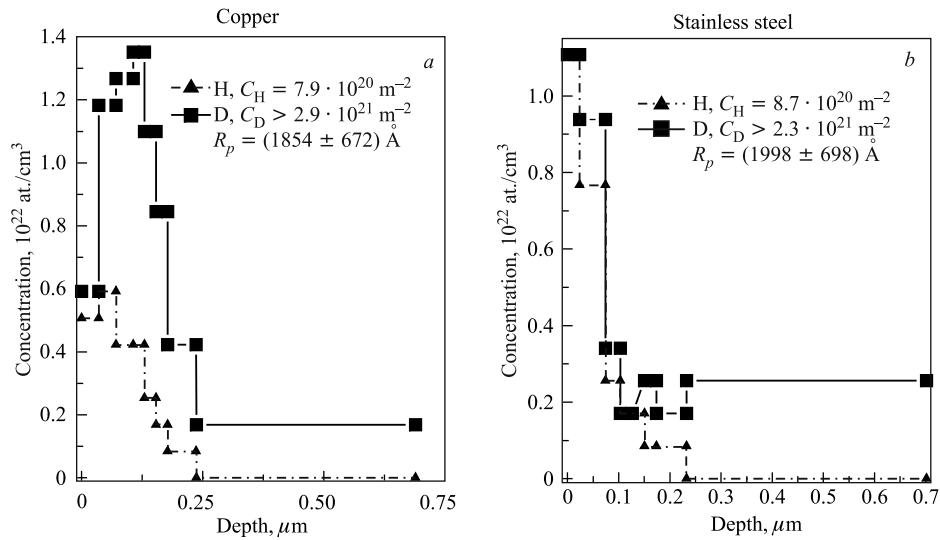


Fig. 5. The depth profiles of D and H atoms after 25-keV  $\text{D}^+$  implantation at one fluence  $\Phi_2 = 1.5 \cdot 10^{22} \text{ m}^{-2}$  in Cu (a) and stainless steel  $\text{Fe}_{72}\text{Cr}_{18}\text{Ni}_{10}$  (b) samples

2.1.5. *Implantation to Vanadium Targets.* Very interesting results were obtained by the ERDA studies of vanadium foils implanted by  $D^+$  ions for all the studied fluences. The total concentrations of D atoms in implanted pure V and Pd and  $Pd_{0.9}Rh_{0.1}$  alloy samples are presented in Figs. 6 and 7 for comparison.

The irradiated surfaces of V and Pd samples implanted by  $D^+$  ions at a fluence  $\Phi_{\max} = 2.3 \cdot 10^{22} \text{ m}^{-2}$  became dark brown and dark blue, respectively.

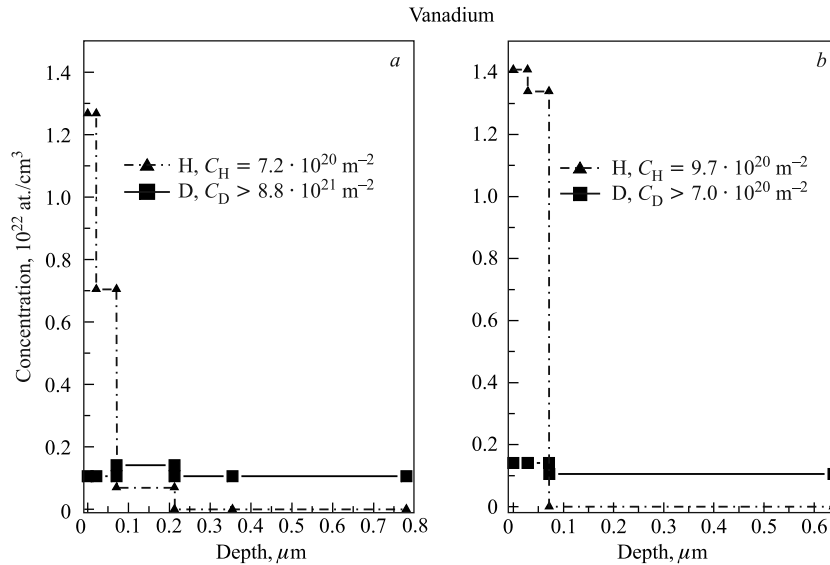


Fig. 6. The depth concentrations of D and H atoms in V samples after 25-keV  $D^+$  implantation at two fluences:  $\Phi_2 = 1.5 \cdot 10^{22} \text{ m}^{-2}$  (a) and  $\Phi_{\max} = 2.3 \cdot 10^{22} \text{ m}^{-2}$  (b). The  $D^+$  projected range is  $R_p = (1955 \pm 571) \text{ \AA}$

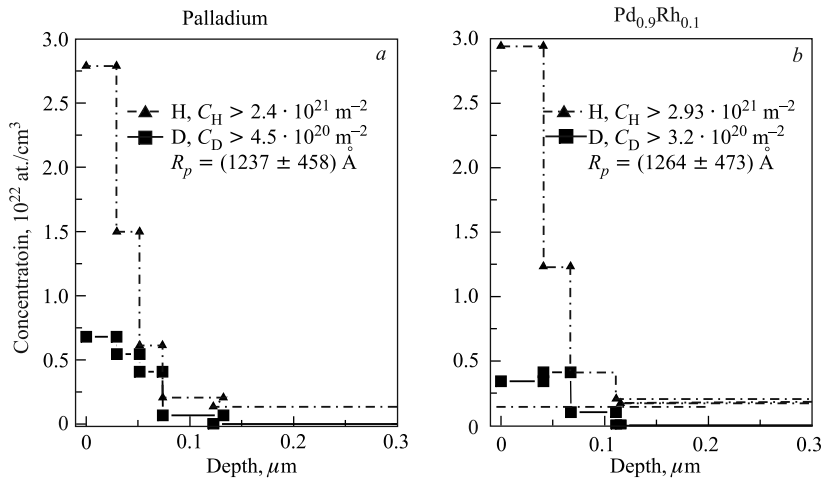


Fig. 7. The depth concentrations of D and H atoms after 25-keV  $D^+$  implantation at fluence  $\Phi_1 = 1.2 \cdot 10^{22} \text{ m}^{-2}$  in pure Pd (a) and  $Pd_{0.9}Rh_{0.1}$  (b) samples

The calculated D/V and D/Pd ratios for fluences of implantation  $\Phi_{\max} = 2.3 \cdot 10^{22} \text{ m}^{-2}$  and  $\Phi_1 = 1.2 \cdot 10^{22} \text{ m}^{-2}$  (3) have values  $n_V^{\max}(\text{D}^+) = 2.06 \text{ at. D/at. V}$  and  $n_{\text{Pd}}^{\max}(\text{D}^+) = 1.69 \text{ at. D/at. Pd}$ , respectively. The total concentrations and depth concentrations of implanted  $\text{D}^+$  ions are very low. The measured values of D concentrations in both V and Pd implanted foils are less than 1–2% only; i.e., these values are near the detection limit of the employed ERDA setup.

It is known that Pd foils can be used as superfilters of hydrogen isotopes and impermeable membranes for other gases [7, 14, 15, 18, 20, 24–26]. The conclusion of our studies is that V foils can also be used as selective membranes for purification of hydrogen isotopes from other gases. It was shown [26] that with the use of so-called atomizer, i.e., special heating element (1000–2300 K temperature range) which allows one to cause dissociation of molecular hydrogen and its heavier isotopes (chemical reaction  $\text{H}_2/\text{D}_2/\text{T}_2 \rightarrow \text{H} + \text{H/D} + \text{D/T} + \text{T}$ ), the membranes made of vanadium together with niobium can also purify hydrogen. Experiments on vanadium-assisted gas separation began only recently. To our knowledge, no publications are devoted to investigation of desorption of high amounts of hydrogen-deuterium atoms after high-dose implantation.

All experimentally measured values for D-atom total concentrations in the studied materials such as Zr, Ti, V, Cu, Pd, SS and  $\text{Al}_2\text{O}_3$  are summarized in Table 2. It is important to note that the sputtered layers in all the studied metals and alloys are very thin (about 10–20 Å) in comparison to the projected range of  $\text{D}^+$  ions. As can be seen from Table 2, there is a close relation between experimentally measured total concentrations and implanted ion fluences, though a large spread of experimental profiles is observed in metals and alloys targets. Some positions from Table 2 are not filled yet and there are some inconsistencies to be settled in the very near future.

**Table 2. Total measured concentrations of implanted deuterium in several metals and alloys at various fluences**

| Fluence of $\text{D}^+$ ion implantation, $10^{22} \text{ m}^{-2}$ | $\Phi_1 = 1.2$   | $\Phi_2 = 1.5$   | $\Phi_3 = 1.8$   | $\Phi_{\max} = 2.3$  |
|--|--|--|--|--|
| Zirconium, Zr  | —  | $> 1.5 \cdot 10^{22} \text{ m}^{-2}$<br>No desorption    | $\approx 1.5 \cdot 10^{22} \text{ m}^{-2}$<br>No desorption    | $\sim 2.3 \cdot 10^{18} \text{ cm}^{-2}$<br>No desorption      |
| Titanium, Ti   | —  | —  | $> 0.6 \cdot 10^{22} \text{ m}^{-2}$<br>Desorption (?)         | $> 0.65 \cdot 10^{22} \text{ m}^{-2}$<br>Desorption (?)        |
| Copper, Cu   | —  | $> 2.9 \cdot 10^{21} \text{ m}^{-2}$<br>Desorption (?)   | —  | —  |
| Palladium, Pd  | $> 4.5 \cdot 10^{20} \text{ m}^{-2}$<br>Super H/D filter | —  | —  | —  |
| Vanadium, V  | —  | $< 8.8 \cdot 10^{20} \text{ m}^{-2}$<br>Super H/D filter | $\approx 4.4 \cdot 10^{20} \text{ m}^{-2}$<br>Super H/D filter | $\approx 7.0 \cdot 10^{20} \text{ m}^{-2}$<br>Super H/D filter |
| Stainless steel, $\text{Fe}_{72}\text{Cr}_{18}\text{Ni}_{10}$      | —  | $> 2.3 \cdot 10^{21} \text{ m}^{-2}$<br>Desorption (?)   | —  | —  |
| $\text{Al}_2\text{O}_3$  | —  | —  | —  | $> 6.4 \cdot 10^{22} \text{ m}^{-2}$<br>Desorption (?)         |

Capability of pure Pd for dissolving significant amounts of hydrogen was discovered a long time ago (1888, see [7, 15]). Since that time detailed investigations of hydrogen behavior in Pd alloys (in particular, with noble metals) attract considerable applied and fundamental interest. The D and H depth profiles in several Pd alloys were measured by ERDA repeatedly: the first measurement within 10 days and 3 months after the implantation (Fig. 8) (see also Fig. 7 for depth profiles for Pd and Pd<sub>0.9</sub>Rh<sub>0.1</sub> alloy). From Fig. 8 one can conclude that the concentrations of implanted D atoms remain virtually unchanged. Some differences between the measured values can be connected also with different energies of ERDA setups at FLNP–JINR and at SINP-MSU: 2.3 and 1.9 MeV, respectively. It is necessary to note that the observations of high H concentration at great depth should be verified. The retention of high total concentrations of D atoms in measured Pd and Pd alloys can be explained by absorption of D atoms in gas bubbles and at grain boundaries [9–13].

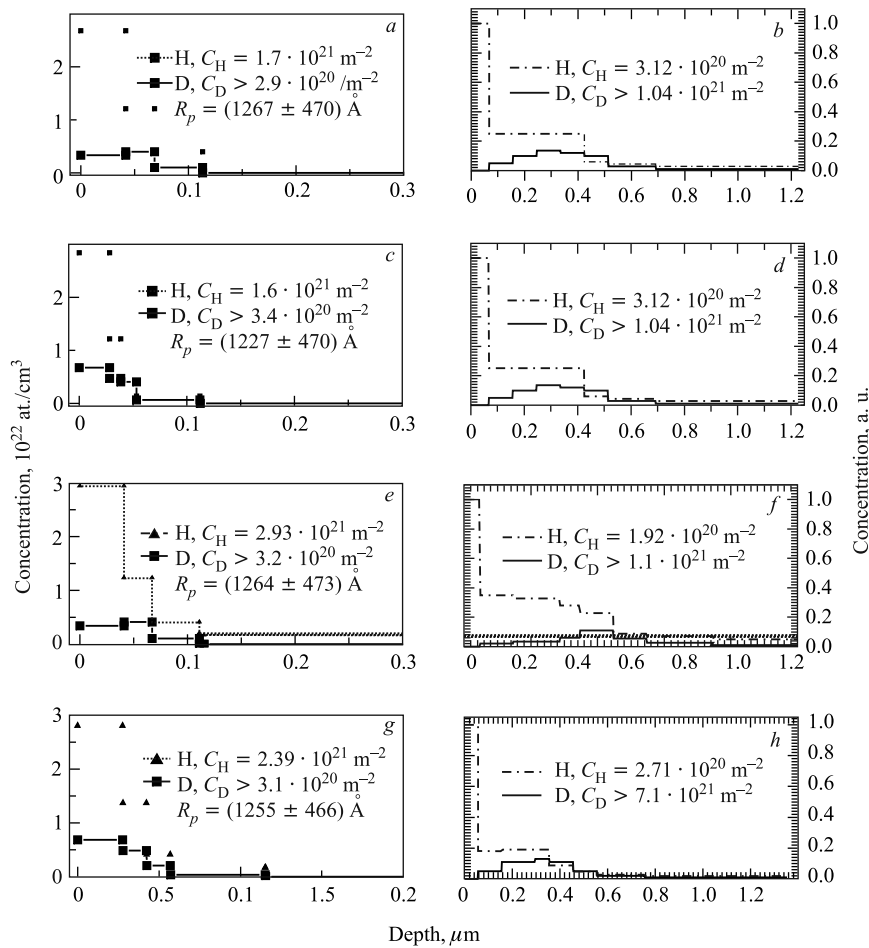


Fig. 8. The depth profiles of D and H atoms after 25-keV D<sup>+</sup> implantation at fluence  $\Phi_1 = 1.2 \cdot 10^{22} \text{ m}^{-2}$  in the following samples: Pd<sub>0.9</sub>Ag<sub>0.1</sub> (a, b); Pd<sub>0.9</sub>Pt<sub>0.1</sub> (c, d); Pd<sub>0.9</sub>Rh<sub>0.1</sub> (e, f); Pd<sub>0.9</sub>Ru<sub>0.1</sub> (g, h). The left column — 10 days; the right column — 3 months after the implantation

Table 3. Total concentrations of D (top value) and H atoms (bottom value) for all the studied palladium alloys: Pd<sub>0.9</sub>Ag<sub>0.1</sub>, Pd<sub>0.9</sub>Pt<sub>0.1</sub>, Pd<sub>0.9</sub>Ru<sub>0.1</sub>, and Pd<sub>0.9</sub>Rh<sub>0.1</sub> at fluence  $\Phi_1 = 1.2 \cdot 10^{22} \text{ m}^{-2}$

| Total concentrations   | Pure Pd  | Pd <sub>0.9</sub> Ag <sub>0.1</sub> | Pd <sub>0.9</sub> Pt <sub>0.1</sub> | Pd <sub>0.9</sub> Ru <sub>0.1</sub> | Pd <sub>0.9</sub> Rh <sub>0.1</sub> |
|--|--|-------------------------------------|-------------------------------------|-------------------------------------|-------------------------------------|
| $\rho, \text{ g/cm}^3$   | 12.02  | 11.87                               | 12.96                               | 12.05                               | 12.03                               |
| $N, 10^{22} \text{ at. M/cm}^3$  | 6.803  | 6.798                               | 6.770                               | 6.854                               | 6.803                               |
| Implantation of deuterium ions, energy 25 keV, fluence $\Phi_1 = 1.2 \cdot 10^{22} \text{ m}^{-2}$ |  |                                     |                                     |                                     |                                     |
| $R_p^D, \text{ \AA}$   | $1237 \pm 458$   | $1267 \pm 470$                      | $1227 \pm 470$                      | $1255 \pm 466$                      | $1264 \pm 473$                      |
| $S, \text{ at. M/at. D}$   | 0.00112  | 0.0104 (Pd)<br>0.00086 (Ag)         | 0.0083 (Pd)<br>0.00062 (Pt)         | 0.0073 (Pd)<br>0.00084 (Ru)         | 0.00074 (Pd)<br>0.00098 (Rh)        |
| Equation (2)   | $n(D^+) \approx 1.42 \text{ at. D}^+/\text{at. M}$ at depth $\approx 1450 \text{ \AA}$ |                                     |                                     |                                     |                                     |
| ERDA measurements after implantation (FLNP–JINR, He <sup>+</sup> — 2.3 MeV)                        |  |                                     |                                     |                                     |                                     |
| $R_p^{\text{He}}, \mu\text{m}$   | $0.88 \pm 0.30$  | $0.89 \pm 0.30$                     | $0.88 \pm 0.32$                     | $0.87 \pm 0.30$                     | $0.88 \pm 0.28$                     |
| $C_D, 10^{21} \text{ m}^{-2}$  | $\sim 0.45$  | $\sim 0.29$                         | $\sim 0.34$                         | $\sim 0.31$                         | $\sim 0.29$                         |
| $C_H, 10^{21} \text{ m}^{-2}$  | $> 2.41$   | $> 1.70$                            | $> 1.57$                            | $> 2.39$                            | $> 3.21$                            |
| ERDA measurements two month later after implantation (MSU, He <sup>+</sup> — 1.9 MeV)              |  |                                     |                                     |                                     |                                     |
| $C_D, 10^{21} \text{ m}^{-2}$  | —  | $\sim 0.20$                         | $\sim 0.31$                         | $\sim 0.27$                         | $\sim 0.19$                         |
| $C_H, 10^{21} \text{ m}^{-2}$  | —  | $> 1.10$                            | $> 1.04$                            | $> 0.71$                            | $> 1.10$                            |

Table 3 summarizes the ERDA results for total D and H concentrations in Pd and in some palladium-based alloys as: Pd<sub>0.9</sub>Ag<sub>0.1</sub>, Pd<sub>0.9</sub>Pt<sub>0.1</sub>, Pd<sub>0.9</sub>Ru<sub>0.1</sub>, and Pd<sub>0.9</sub>Rh<sub>0.1</sub>. We repeat here some main results: from comparison of Tables 1 and 2 it is clear that the concentrations of implanted deuterium and of intrinsic hydrogen do not change much for a long period (three months) between the measurements. Minor differences are most probably related by different experimental setups for ERDA study and different energies of employed He<sup>+</sup> ions beams at FLNP (JINR, Dubna) and at SINP (MSU, Moscow). It is necessary to note that the depth distributions of intrinsic hydrogen atoms are very deep and have high concentrations for all Pd alloys. We conclude that both isotopes — D and H atoms — exist in alloy lattices as substitutional and interstitial atoms and/or as small gas bubbles [9–13]. The obtained hydrogen concentrations are high:  $(1.5\text{--}3.2) \cdot 10^{21} \text{ m}^{-2}$ , which is very promising for possible future applications. The depth distribution of intrinsic H atoms in all the studied Pd alloys was very broad.

**2.2. Small-Angle X-ray Scattering.** The small-angle scattering intensity for almost all the studied foils was negligible, which indicates high homogeneity of the electron density distribution in the samples. This can be easily interpreted as absence of extended defects and/or of clustering of point defects. However, in the corundum and titanium samples the SAXS signal was observed. The size distribution curves of spherical scatterers for these samples are shown in Fig. 9. Scattering from initial (unimplanted) samples was used as a background, thus permitting one to minimize any possible contribution from intrinsic defects and/or from texture.

The scattering patterns for these two samples are very different. The scatterers in Al<sub>2</sub>O<sub>3</sub> produced by implantation of 25-keV D<sup>+</sup> ions up to a dose of  $\Phi_{\text{max}} = 2.3 \cdot 10^{22} \text{ m}^{-2}$  can be described as a monodisperse system with diameters close to 1 nm. Such a narrow size

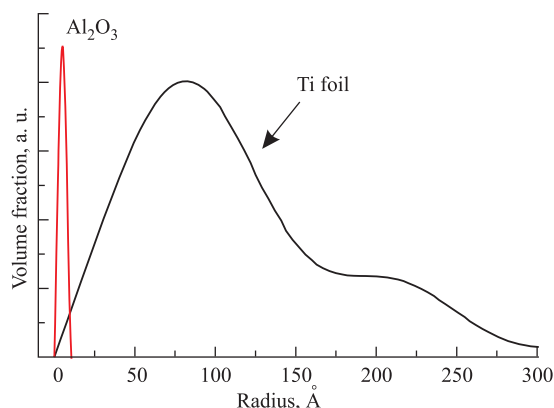


Fig. 9. Size distribution of scatterers in ion implanted titanium and corundum

distribution is not very common for inorganic systems. Most likely, this scattering is due to small gas bubbles or similar defects. However, in titanium sample the size distribution of the scatterers is very different: it is broad with a main peak around 10 nm (radius) and secondary one around 16 nm. Unique assignment of these peaks using only SAXS data is impossible. The scattering could be assigned to clusters of point, e.g., radiation, defects. They might be precursors of bubbles, or reflect formation of hydride phase.

The SAXS data might be explained by very different behavior of hydrogen in metals and ceramics. In metals hydrogen is present as a «lattice gas» or form hydrides. In ceramics hydrogen may form point defects saturating dangling bonds, it can recombine to  $H_2$  molecule, etc. In addition, the diffusion rates of H isotopes are much higher in metals, thus explaining high desorption rates.

It is well known [9–12, 22, 23] that deuterium and helium confined in small bubbles in metals with high mechanical strength can be present in solid state. The internal pressure should be about  $P = 2\gamma/R$ , where  $\gamma$  is a surface tension. The estimated values of He pressure in bubbles in aluminum and nickel is  $P \approx 13$  MPa (radius of the bubble is  $R = 0.65$  nm with atomic density  $\approx 1.4 \cdot 10^{23}$  He/cm<sup>3</sup>) and  $P \approx 50$  GPa (with atomic density  $\approx 1.4 \cdot 10^{23}$  He/cm<sup>3</sup>), respectively [12, 13, 22, 23].

## CONCLUSIONS

The depth distributions of D and H atoms after implantation of  $D^+$  into several pure metals (Zr, Ti, Cu, V, and Pd), alloys (SS, Pd<sub>0.9</sub>Ag<sub>0.1</sub>, Pd<sub>0.9</sub>Pt<sub>0.1</sub>, Pd<sub>0.9</sub>Ru<sub>0.1</sub>, and Pd<sub>0.9</sub>Rh<sub>0.1</sub>) and single crystal Al<sub>2</sub>O<sub>3</sub> were measured using ERDA method.

It is shown that total concentrations of implanted deuterium for high fluences  $\Phi = 1.2 \cdot 10^{22}$ ,  $1.5 \cdot 10^{22}$ ,  $1.8 \cdot 10^{22}$ , and  $2.3 \cdot 10^{22}$  m<sup>-2</sup> correspond to employed ion fluences, in particular for Zr foils. The observed depth profiles of deuterium show a spread along the projected range of incident ions.

The  $D^+$  implantation up to very high fluences with small ion flux  $\approx 3.5 \cdot 10^{17}$  m<sup>-2</sup> · s<sup>-1</sup> allowed us to obtain high total concentrations in most of the studied metals and alloys, except for V and Pd. Deuterium-saturated layers span considerable depth, several times the projected implantation ranges. No blistering and exfoliation was observed.

High desorption losses of deuterium were observed for implanted vanadium samples for all the used fluences. The comparison of implanted samples of V and Pd allowed us to conclude that V foils can be used together with more expensive Pd foils for separation and purification of hydrogen and its heavier isotopes from other gases.

In future it is important to study other deuterium-implanted elements of group V of the Periodic Table such as Nb and Ta. Vanadium is known to have lower level and shorter period of fission fragment radioactivity decays than heavier elements of group V, so this metal is much better suited for applications in fusion reactors.

Desorption of implanted deuterium, as well as its spread, is very small for Pd and its diluted alloys. These samples also contain high concentrations of intrinsic hydrogen.

The metal surfaces change color once a certain critical fluence value is surpassed. The extent of the changes is proportional to implantation fluence. This allows us to estimate the implantation fluence at least semi-quantitatively, e.g., using spectrophotometer.

All the implanted metal samples were deformed, probably by emergence of gas pores or gas bubbles.

Small-angle X-ray scattering (SAXS) reveals the appearance of small well-defined heterogeneities with radii approx. 1 nm in implanted corundum. These defects might correspond to gas bubbles. Heterogeneities also appear in implanted titanium, though the size distribution is much broader and the defects are much larger ( $> 10$  nm). These scatterers might represent early stages of bubbles formation or agglomeration of point defects. No SAXS signal was detected for the other implanted samples, indicating the absence of defects clusterization.

**Acknowledgements.** The authors are grateful to Prof. Andrzej Czachor (Atomic Energy Institute POLATOM, Świerk/Otwock, Poland) for the provision of the Pd and Pd-based alloy materials for the studies and fruitful discussions in all the stages of the studies, and to Prof. Stanislaw Filipek (Institute of Chemical Physics, Warsaw, Poland) for the provision of a high-pressure setup for metals and alloys saturations.

#### REFERENCES

1. Winter C. J., Nitsch J. Hydrogen as an Energy Carrier: Technologies, Systems, Economy. Springer, 1988.
2. Schlappbach L., Zuttel A. Hydrogen-Storage Materials for Mobile Applications // Nature. 2001. V. 414. P. 353–361.
3. Zuttel A. Materials for Hydrogen Storage // Materials Today. 2003. V. 6. P. 24–33.
4. Zaluski L., Zaluska A., Strom-Olsen J. O. Nanocrystalline Metal Hydrides // J. Alloys and Compounds. 1997. V. 253–254. P. 70–79.
5. Miyamoto K. Fundamentals of Plasma Physics and Controlled Fusion. M.: Fizmatlit, 2007. 424 p.
6. Mikhailov V. N. et al. Lithium for Fusion Reactors and Space Nuclear Power Systems of the 21st Century. M.: Energoatomizdat, 1999. 527 p.
7. Metal Hydrides as Materials of Nuclear Reactions / Eds. W. M. Mueller, J. P. Blackledge, G. G. Libowitz. New York; London, 1968. P. 58–83.
8. Bauer W. Surface Processes in Plasma Wall Interactions // J. Nucl. Mater. 1978. V. 76/77. P. 3–15.
9. Smith D. L. Sputtering Model for Fusion Reactor First-Wall Materials // J. Nucl. Mater. 1978. V. 75. P. 20–31.

10. *Johnson P. B., Mazey D. J.* Helium-Bubble Superlattice in Copper and Nickel // *Nature*. 1979. V. 281(5730). P. 359–360.
11. *Johnson P. B., Mazey D. J.* The Gas-Bubble Superlattice and the Development of Surface Structure in  $\text{He}^+$  and  $\text{H}^+$  Irradiated Metals at 300 K // *J. Nucl. Mater.* 1980. V. 93/94. P. 721–727.
12. *Kalin B. A., Chernov I. I.* Lattice Organization of Pore and Bubble Structure in Irradiated Metals and Alloys // *Atomic Science Abroad*. 1986. V. 10. P. 3–9.
13. *Jager W., Roth J.* Microstructure of Ni and Stainless Steel after Multiple Energy He and D Implantation // *J. Nucl. Mater.* 1980. V. 93/94. P. 756–766.
14. *Wiśniewski R.* High Pressure Apparatus for Gaseous Hydrogen up to 25 Kilobars and Temperature Range  $-50^\circ\text{C}$  to  $+100^\circ\text{C}$  // *Rev. Sci. Instr.* 1970. V. 41(3). P. 455–464.
15. *Baranowski B., Filipek S. M.* 45 Years of Nickel Hydrides // *Polish J. Chem.* 2005. V. 79. P. 789–806; <http://malina.inchf.edu.pl/person/filipek.html>.
16. *Didyk A. Yu. et al.* Studies of Radiation Effects in Materials on ECR Heavy Ion Source Beam Line at FLNR // *Proc. of XI Intern. Conf. «Radiation Physics of Solids»*, Sevastopol, Crimea, Ukraine, July 2001. 2001. P. 340–350.
17. *Biersack J. P., Haggmark L. G.* A Monte Carlo Computer Program for the Transport of Energetic Ions in Amorphous Targets // *Nucl. Instr. Meth. B*. 1980. V. 174. P. 257–269; <http://www.srim.org>.
18. *Wiśniewski R., Rostockil A. J.* Hall Effects in Pd–H System // *Phys. Rev. B*. 1971. V. 3. P. 251–252.
19. *Hrubčín L. et al.* Application of the ERD Method for Hydrogen Determination in Silicon (Oxy)Nitride Thin Films Prepared by ECR Plasma Deposition // *Nucl. Instr. Meth. B*. 1994. V. 85. P. 60–62.
20. *Ishigami R., Ito Y., Yasida K.* In Situ ERDA Measurements of Hydrogen Isotope Concentrations in Palladium at Atmospheric Pressure // *Nucl. Instr. Meth. B*. 2008. V. 266. P. 1319–1323.
21. *Borisov A. M. et al.* Peculiarities of Impulse Polyenergetic Implantation // *Izv. Rus. Acad. Sci. Series Physics*. 2000. V. 64(4). P. 763–766.
22. *Komarov F. F.* Ion Implantation to Metals. M.: Metallurgy, 1990. 216 p. (in Russian).
23. *Jager W. et al.* // *Rad. Effects*. 1983. V. 78. P. 315–325.
24. *Klevtsov V. G. et al.* Diffusion Cleaning of Hydrogen Isotopes by Palladium Filters // *Hydrogen Isotopes. Fundamental and Applied Research: Collection of Papers* / Ed. A. A. Uchimchyk. Sarov, 2009. P. 360–365.
25. *Uchimchyk A. A., Gaevoj V. K.* Studies of Hydrogen Isotope Permeability through Some Constructive Materials // *Ibid.* P. 330–335.
26. *Musjaev R. N. et al.* Study of Superpermeability Phenomenon of Hydrogen Isotopes through Vanadium Membrane on PROMETEI Setup // *Ibid.* P. 355–359.
27. *Chernyshov A. A., Veligzhanin A. A., Zubavichus Y. V.* Structural Materials Science End-Station at the Kurchatov Synchrotron Radiation Source: Recent Instrumentation Upgrades and Experimental Results // *Nucl. Instr. Meth. A*. 2009. V. 603. P. 95–98.
28. *Svergun D. I.* Determination of the Regularization Parameter in Indirect-Transform Methods Using Perceptual Criteria // *J. Appl. Cryst.* 1992. V. 25. P. 495–503.

Received on March 21, 2011.